Fibre orientation near a wall of a headbox

By Allan Carlsson[†], L. Daniel Söderberg[†,‡] & Fredrik Lundell[†]

[†]Linné Flow Centre, KTH Mechanics, SE - 100 44 Stockholm, Sweden
[‡]STFI-Packforsk AB, SE - 114 86 Stockholm, Sweden

Experimental results on the fibre orientation in a laboratory scale headbox are reported. A steerable filter was used to determine the orientation of bleached unbeaten birch fibres at different distances from one of the inclined walls of the headbox contraction. Due to optical limitations only dilute suspensions were studied. It is shown that the fibre orientation distribution varies with the distance from the wall. Sufficiently far upstream in the headbox a more anisotropic distribution is found closer to the wall as compared to farther away from the wall.

1. Introduction

The mechanical properties of a paper sheet are highly dependent on the orientation distribution of fibres. The fibre orientation in the network structure is determined by the headbox and initial dewatering process, *i.e.* in the forming section of the paper machine. The main function of the headbox is to transform a pipe flow, with a diameter of about 0.8 m, into a free jet with a width of about 10 m and a thickness of 0.01 m. Due to the contraction in the nozzle of the headbox the suspension is accelerated and the positive rate-of-strain in the machine direction (MD) will tend to align the fibres with the flow direction. This orientation is often reflected in the final paper sheet, where most fibres are oriented in MD. It should be mentioned that the orientation is also affected by the dewatering process after the headbox. The free jet leaving the headbox impinges on one or between two permeable bands called wires. The water is drained through the wires resulting in a rapid increase of the suspensions fibre concentration. In an experimental study by Nordström (2003*b*) it was shown that the velocity difference between the jet and the moving wires have an effect on the fibre orientation. A larger velocity difference, both positive and negative, results in a more anisotropic paper sheet, *i.e.* more fibres oriented in MD. A smaller velocity difference, on the other hand, results in a more isotropic orientation distribution.

Some recent attention has been given to the fibre dynamics inside a headbox. The orientation distribution has been measured experimentally at the

outlet of a headbox nozzle, Ullmar (1998). It was shown that increasing the headbox contraction rate resulted in higher anisotropy values. Furthermore, it was concluded that the flow rate through the headbox had a very small effect on the orientation distribution. Nordström (2003*a*) also reported that the effect of the flow rate on the fibre orientation in the final paper sheet was small.

A qualitative agreement with experimental data, concerning the orientation state of fibres in a headbox, was found analytically, Olson (1998), by neglecting effects of turbulence. The change of the orientation distribution in turbulent flows can be modeled with a Fokker-Planck type of equation, *e.g.* Krushkal & Gallily (1988) and Olson & Kerekes (1998). This has been done with application to headboxes by *e.g.* Olson *et al.* (2004), Brown (2005), Parsheh, Brown & Aidun (2005, 2006*a*,*b*) and Hyensjö *et al.* (2007). An accurate reproduction of experimental results has been obtained in these studies. In order to attain good results in these computations knowledge of turbulence quantities, in particular the turbulence intensity level at the inlet, is a prerequisite.

Nordström (2003*b*) showed that the orientation distribution is non-uniform over the thickness (Z) of the paper sheet. The sheet is generally more anisotropic in the core than on both sheet surfaces. This is also indicated in experimental measurements on the fibre orientation in a headbox jet by Asplund & Norman (2004). Along the centreline of the headbox a solid vane was inserted and in a region behind the vane the anisotropy was reduced. Aidun & Kovacs (1995) made a computational investigation and suggested that the main cause of a non-uniform fibre orientation in the cross dircetion (CD) is the secondary flows generated in the headbox due to the boundary layer formation along the side walls of the nozzle.

The present study aims at further investigating the wall influence on the fibre orientation. In many industrial headboxes a set of vanes are implemented as solid flow dividers in the headbox, mainly for the reason of damping out large scale motions that can lead to a bad paper formation. Boundary layers will form along all these vanes. The thickness of these boundary layers is of the order of 0.001 m. Considering that the thickness of the jet leaving the headbox is of the order 0.01 m a large fraction of the suspension is influenced by the boundary layers in the headbox. The vanes could therefore potentially have a large impact on the orientation distribution of fibres leaving the headbox and consequently also on the distribution in the final paper sheet.

Some attention has been given to the wall effect on the motion of fibres. For instance numerical studies have been performed by Hsu & Ganatos (1989, 1994), Gavze & Shapiro (1997) and Pozrikidis (2005). Experimental studies have also been done by Stover & Cohen (1990), Moses, Advani & Reinhardt (2001), Holm & Söderberg (2007) and Carlsson, Lundell & Söderberg (2007). These studies all have in common that they have been focusing on laminar viscous flow. There is still a lack of experimental data on near wall fibre

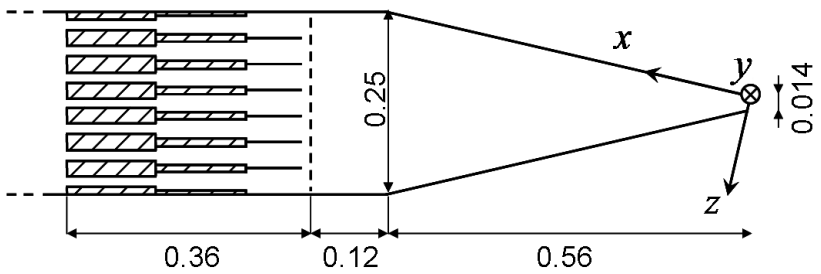

FIGURE 1. Schematic of the headbox with a coordinate system origininating at contraction outlet. Measures are in m.

orientation in flows where intertial effects can not be neglected. In this study the fibre orientation is measured along one of the walls of a laboratory scale headbox. Some preliminary results on practically the same experimental setup have been reported earlier in Carlsson, Söderberg & Lundell (2008).

2. Experimental section

2.1. *Apparatus*

A schematic of the headbox used is shown in figure 1. The same headbox was used in earlier studies by *e.g.* Ullmar (1998), Asplund & Norman (2004) and Carlsson *et al.* (2008), and consists of a tube bank and a contraction. In order to get optical access to the flow the walls are made of acrylic. The tube bank is divided in three sections; two circular and one square section. The contraction ratio R, defined as the ratio between the height at the contraction inlet divided with the height of the channel, is $R \approx 17$ at the outlet. A coordinate system is defined in the figure, where x runs upstream along the direction of the upper wall of the contraction and $x = 0$ where the parallel section begins. The wall normal distance to the upper wall is denoted by z.

To visualize the flow a CCD camera (Prosilica GE680) with a lens of focal length 50 mm (Fujinon HF50HA-1B) was mounted above the wall at fixed x-positions. An extension tube was used in order to limit the field of view to approximately 1 cm^2. The camera was placed to capture images parallel to the wall in the centre of the channel in the spanwise direction (y), *i.e.* about 5 cm from both side walls.

To illuminate the field of view a light sheet was generated. The setup is sketched in figure 2. A monochromatic light beam ($\lambda = 532$ nm), with an output power of the order 340 mW, is generated by a laser (Laserglow Technologies/Hercules - 325). The beam diameter is less than 1.5 mm and the full angle beam divergence is about 1 mrad which results in a diameter of about 2 mm at the position of the headbox. The beam is traversed to the desired z-position by an adjustable inclination of a 6 mm thick glass plate. A cylindrical

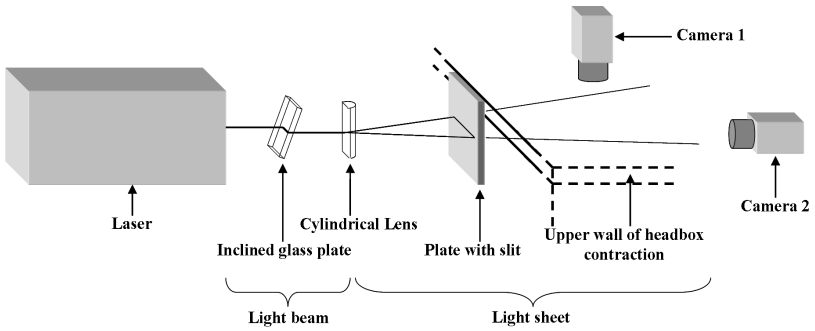

FIGURE 2. Schematic of the light sheet generation and camera positions.

lens of focal length 10 mm transforms the beam into a sheet parallel to the headbox wall. In order to reduce the thickness of the sheet it passes a slit with a thickness of 0.5 mm before entering the headbox. The slit can be traversed in the vertical direction with an accuracy of 0.01 mm. On the other side of the headbox a second camera is mounted in order to determine the centre position of the sheet in relation to the wall. This is done with an accuracy of about 0.1 mm. The thickness of the sheet as it exits the headbox is estimated to be around 2 mm. A linear interpolation gives a thickness of about 1.3 mm in the centre of the channel where the fibre orientation is studied. It should also be mentioned that the light intensity is not constant across the light sheet. The intensity is higher towards the centre of the sheet and as a consequence fibres are more easily detected near the centre of the sheet.

2.2. *Suspension*

A bleached unbeaten birch suspension was used in the study. A sample of the suspension was analyzed with L&W Fiber Tester. The probability density function (PDF) of the length of fibres is shown in figure 3. The arithmetic mean of the fibre length is $l_m \approx 0.7$ mm and the mean fibre width is $w_m \approx 18$ μm. The mass concentration of fibres was $c_m \approx 3 \cdot 10^{-5}$.

Another way to denote the concentration of a suspension is to use nl^3, where n is the number density of fibres and l is a typical fibre length. The main reason for using this expression is that it is a better indicator of how frequent fibre-fibre interactions are than the mass concentration. Sometimes a crowding factor N is introduced for the same reason, see Kerekes & Schell (1992), where N only differs from nl^3 by a numerical factor, $N = \pi nl^3/6$. When $nl^3 << 1$ the suspension is generally considered dilute, *e.g.* Sundararajakumar & Koch (1997), and fibre-fibre interactions can usually be neglected. When $nl^3 = O(1)$ hydrodynamic fibre-fibre interactions occurs more frequently and

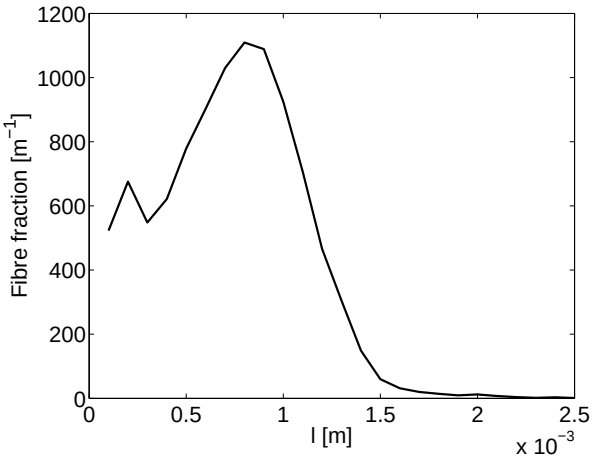

FIGURE 3. Length distribution of fibres in the suspension.

generally cannot be neglected. Eventually, if the concentration is increased even further, mechanical interactions between fibres also have to be considered.

In order to compute nl^3 the approximate relation $nl^3 \approx 1000 c_m l^2/k$ is used, where the density of the suspended fibres is estimated to be about 1000 kg/m^3. With a fibre coarseness of $k \approx 100$ μg/m the concentration in the experiments is estimated to be $nl^3 \approx 0.15$. In industrial headboxes the concentration is typically between $c_m = 10^{-3}$ and 10^{-2} or $nl^3 \approx 5$ and 50, for suspensions with similar fibres as used in the present experiments. Consequently fibre-fibre interactions could have an effect on the fibre dynamics in the headbox of a paper machine, but are not expected to significantly influence the results in the present experiments.

2.3. *Measuring and analyzing procedure*

The fibre orientation and velocity were studied in planes parallel to the upper solid wall of the headbox at three different x-positions ($x = 0.09$, 0.25 and 0.45 m). These x-positions correspond to contraction ratios of $R = 4.9$, 2.1 and 1.3. At each x-position the centre of the laser sheet was traversed to five z-positions ($z = 0.5$, 1.0, 1.5, 2.0 and 5.0 mm). Analyzing the images from camera 2, showing the light sheet as it exits the headbox, has revealed an unintended offset of 0.25 mm in z for $x = 0.45$ m. This mistake results in that the z-positions, for $x = 0.45$ m, have to be corrected to $z = 0.25$, 0.75, 1.25, 1.75 and 4.75 mm. The value of z denotes the centre of the sheet where the light intensity is at its maximum. Recall that the light sheet is slightly thicker than 1 mm. This means that for the z-position closest to the wall a part of the

sheet is cut off by the wall. Consequently, the centre of the remaining light, illuminating only the fluid, will be slightly farther away from the wall than the reported z, where the light intensity is at its maximum. Therefore, the most appropriate value of z to report closest to the wall is not perfectly clear. In this context it should also be kept in mind that since the light intensity is not constant across the sheet it is more likely to detect a fibre close to the actual centre of the sheet, than anywhere else in the sheet, with the image analysis process.

To detect the orientation of the fibres in the images, a ridge detector within the class of steerable filters was used, Freeman & Adelson (1991). The particular detector used in this study was derived by Jacob & Unser (2004). The algorithm has been applied to fibre suspension flows and is described and evaluated in Carlsson *et al.* (2007, 2009). In this study the orientation β is analyzed and is defined as the angle from the x-direction in the plane parallel to the solid wall (xy-plane).

For the orientation measurements a total of 3000 images were captured at each (x, z)-position with a frame rate of the camera set low enough in order to get statistically independent images, *i.e.* low enough so that all of the fibres, which are captured in one image, will leave the field of view before the next image is captured. The frame rate ranges from 6 Hz (far upstream, close to wall) to 50 Hz (far downstream, far from wall). For the velocity measurements the frame rate is set to 200 Hz for all (x, z)-positions. Due to the increased velocity downstream it was not possible to obtain the velocity profile at $x = 0.09$ m.

3. Results and discussion

3.1. *Velocity*

The volume flow rate during the experiments was $Q \approx 12.5 \cdot 10^{-3}$ m^3/s, resulting in a jet velocity of 8.7 m/s (520 m/min). In order to get an estimation of the velocity profile near the wall individual fibres were tracked manually. Initially the intention was to use a particle image velocimetry algorithm (PIV) on seeding particles to measure the velocity field in the sheet. However, it was found difficult to attain a series of images good enough in order to use PIV. This could partly be due to that the concentration of seeding particles was slightly too large, but it is believed that the main source for the troubles using PIV is the large range of velocities within the light sheet. This is due to the high shear rate in the near wall region.

To be able to get some information about the velocity some individual fibres where tracked manually. The procedure to do this was to choose and mark a number of fibres in an image and search for these in the subsequent image. This turns out to be a time consuming method and therefore only 20 fibres per (x, z)-position were tracked. Measurements were conducted at $x = 0.25$ and 0.45 m. Admittedly more fibres would have to be tracked in order to

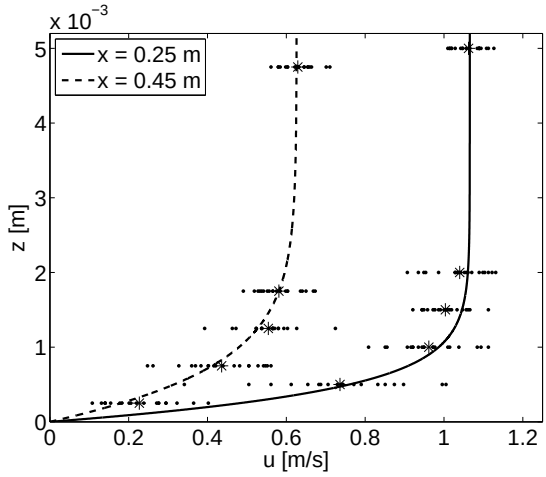

FIGURE 4. Theoretical velocity profiles for $x = 0.24$ m (solid) and $x = 0.45$ m (dashed). The dots and the stars denotes the velocities of individual fibres and the mean of all fibres in each particular serie, respectively.

reach statistical convergence. Still, the velocity measurements are reported to provide an estimation of the velocity gradient and boundary layer thickness near the wall.

The velocity profiles are shown in figure 4. The velocity of each individual fibre is shown as a dot in the figure and the mean value for each (x, z)-position is shown as a star. The solid and dashed lines, denoting the velocity at $x = 0.25$ and 0.45 m, are given by the similarity solution for laminar flow in a two-dimensional convergent channel and can be found in Schlichting (1979). There is a significant scatter in the experimental data. This is in particular seen closest to the wall. It is believed that the scattering mainly reflects the wide range of velocities inside the sheet near the wall. The maximum error in velocity of a tracked fibre is estimated to be ± 0.1 m/s. There are no deviations from the mean value larger than this error for the position farthest away from the wall ($z \approx 5$ mm). Consequently, no conclusions can be drawn directly from the data concerning any velocity fluctuations that may be present in the flow.

The measured mean velocity profile coincides surprisingly well with the similarity solution for laminar flow. A turbulent boundary layer subjected to strong acceleration can return to laminar-like conditions. The acceleration is often quantified by a non-dimensional parameter

$$K = \frac{2\nu \tan \psi}{q}, \tag{1}$$

where ν is the kinematic viscosity of the fluid, ψ is half the contraction angle and q is the flow rate per unit width in the channel. Some studies have been made to find the critical value of K where the onset to relaminarization begins. Among these are Moretti & Kays (1965) who found an apparent re-transition to a laminar boundary layer for $K > 3.5 \cdot 10^{-6}$ and Parsheh (2001) who found the critical K to be about $3.1 \cdot 10^{-6}$. In the present study $K \approx 3.4 \cdot 10^{-6}$ so a relaminarization process is likely to be present. Since, the boundary layer already seems to have reached a profile close to the similarity solution for laminar flow at $x = 0.45$ and 0.25 m it is natural to assume that it will stay close to this solution also farther downstream at $x = 0.09$. From the similarity solution the boundary layer thickness, defined as the distance from the wall where the mean velocity is 0.99 times the velocity far from the wall, is computed to be 0.6, 1.3 and 2.3 mm for $x = 0.09$, 0.25 and 0.45 m, respectively.

3.2. *Fibre orientation distribution*

The number of detected fibres at all (x, z)-positions is shown in table 1. For most positions between 20000 and 40000 fibres are detected, *i.e.* roughly 10 fibres per image. The measurements at different x-positions have been conducted at different times. The suspension has been partly replaced in between the measurements. Although the concentration should be about the same for all measurements it is very approximative, so the absolute numbers should not be compared between different x-positions.

There is a trend for $x = 0.25$ and 0.45 m that more fibres are detected as the distance to the wall is increased. This could possibly reflect an effect of migration towards areas with lower velocity gradients. However, the result should be interpreted with some care. Notable from the number of detected fibres at $x = 0.09$ m is that here there is no clear trend and the numbers differ significantly between the z-positions. For $x = 0.09$ m the boundary layer thickness is about 0.6 mm so the mean flow velocity gradient should be about the same for the four z-positions farthest from the wall. It is also noted that the number of detected fibres at $x = 0.45$ m, $z = 0.25$ mm, in comparison to the other positions, is small. Here it should be recalled that part of the light sheet is cut off by the wall and therefore less fibres are expected to be detected. Still, the number is surprisingly small even if the apparent trend of fewer detected fibres at high velocity gradients is taken into account.

A possible explanation for why so few fibres are detected at $x = 0.45$ m and $z = 0.25$ mm is that fibres close to the wall will undergo a pole vaulting like motion as the sheared fluid will tend to make a fibre rotate. In the rotation of a nearly flow aligned fibre one of the fibre ends hit the wall and the centre of the fibre is pushed away to a position of about half a fibre length from the wall. This kind of motion has been observed in viscous flows by for instance Stover & Cohen (1990). We will see later that most of the fibres are oriented close to the flow direction so the presence of a pole vaulting motion would not

Position	$x = 0.09$ m	$x = 0.25$ m	$x = 0.45$ m
$z^* = 0.5$ mm	34196	24673	9584
$z^* = 1.0$ mm	43142	26542	22354
$z^* = 1.5$ mm	33246	27761	25656
$z^* = 2.0$ mm	35911	38249	25756
$z^* = 5.0$ mm	42340	39568	28033

TABLE 1. The number of detected fibres at all (x, z)-positions. The values of z is given by z^* apart from when $x = 0.45$ m for which $z = z^* - 0.25$ mm.

be surprising. This would for fibres with a length of about 0.7 mm generate a void close to the wall between $z = 0$ and 0.35 mm, where there are few fibres present. Since the centre of the sheet, where the light intensity is highest, is located inside this void when $z = 0.25$ mm this could result in a significant drop in the number of detected fibres.

We will now focus on the fibre orientation near the wall. The distribution of β is shown, for all positions, in figure 5. The distributions at $x = 0.45$, 0.25 and 0.09 m are shown in (a), (b) and (c), respectively. The various lines denote different z-positions. The distributions are a bit coarse and more detected fibres would be desired to get a better convergence. Still, some trends, which will be addressed below, can be deduced from the data.

The perhaps most surprising feature is the asymmetric appearance of the distributions at $x = 0.45$ m in (a). There is at present no clear explanation for this. Similar distributions have been observed in all pre-studies on the setup and was also reported in Carlsson *et al.* (2008). Measurements have also been made in the spanwise direction at $x = 0.45$ m, but no clear difference has been seen as a function of y in these results. The distributions have not appeared to change appreciably in the region of -0.04 m $< y < 0.04$ m at $x = 0.45$ m, where $y = 0$ in the centre of the channel. It is believed that the asymmetric distributions arises due to an asymmetry of the incoming flow. The tube package ends at about 0.25 m upstream from the measurements at $x = 0.45$ m. Farther downstream at $x = 0.25$ m the orientations distributions have developed a more symmetric appearance.

Disregarding the asymmetric feature of the distributions, a clear trend is seen for both $x = 0.45$ and 0.25 m. A more anisotropic distribution is found closer to the wall, *i.e.* the fibres tend to adopt orientations closer to the flow direction ($\beta = 0$) for lower values of z. Possibly velocity fluctuations of the fluid could be of significance here. Fluctuations are most likely to result in a more isotropic fibre orientation distribution, at least if the velocity fluctuations are fairly isotropic in nature. If there are less fluctuations closer to the wall, in the relaminarizing boundary layer, this could result in a more isotropic distribution

farther from the wall. However, it is emphasized that even though the mean velocity profile is close to the laminar profile, it is still likely that turbulent structures remain in the flow, *e.g.* Warnack & Fernholz (1998) and Talamelli *et al.* (2002). Therefore this explanation is not perfectly convincing.

Another possibility that will briefly be presented here is related to the dynamics of fibres in shear flows. As mentioned above a fibre will rotate when the surrounding fluid is sheared. In a viscous flow a fibre is expected to spend most time oriented nearly aligned with the xy-plane during its rotation. It is also likely that most fibres will be relatively close to the flow direction when oriented in this plane. This is what one would expect for fibres rotating in Jeffery orbits, see Jeffery (1922). A fibre will rotate in Jeffery orbits when suspended in a viscous simple shear flow, when all inertial forces are negligible. Clearly it is not straightforward at all to neglect inertial forces in the present study.

Some recent studies have been made on the effect of fluid inertia on the rotation of elongated particles in shear flows, *e.g.* Ding & Aidun (2000), Qi & Luo (2003) and Subramanian & Koch (2005). Two conclusions from these studies is that a weak, but non-negligible fluid inertia, will tend to increase the period of rotation as compared to fibres rotating in Jeffery orbits and fluid inertia will also introduce an orientation drift towards the flow direction. In the present experiments inertial effects are expected to be larger as the distance to the wall is decreased, since the differences in velocity of the fluid over the fibre surface will be greater when the velocity gradient is large. Both conclusions mentioned from the studies on inertial effects should lead to a more aligned distribution near the wall. It is easily realized that a drift in orientation towards the flow direction would lead to a more aligned orientation distribution. Also an increased period due to inertia should lead to a higher anisotropy, since the increased period appears as an increased fraction of time oriented near the xy-plane, where a fibre is likely to be close to the flow direction even when rotating in a Jeffery-like orbit.

Farther downstream at $x = 0.09$ m, shown in figure 5 (c), no clear difference can be seen for different z. The velocity gradient at the wall is increasing downstream so if the reasoning on inertial effects above is significant one might imagine there should be an even larger effect on the fibre orientation at $x = 0.09$ m. Clearly this is not the case.

It should also be recalled that simultaneously, as the velocity gradient at the wall is increased, the boundary layer thickness is decreased in the downstream direction. According to the similarity solution of a planar converging channel the boundary layer thickness should be close to 0.6 mm at $x = 0.09$ m. Consequently large velocity gradients, in the wall normal direction, are only expected to be present for the z-position closest to the wall. It is also worth noticing that at this x-position the boundary layer is thinner than the mean

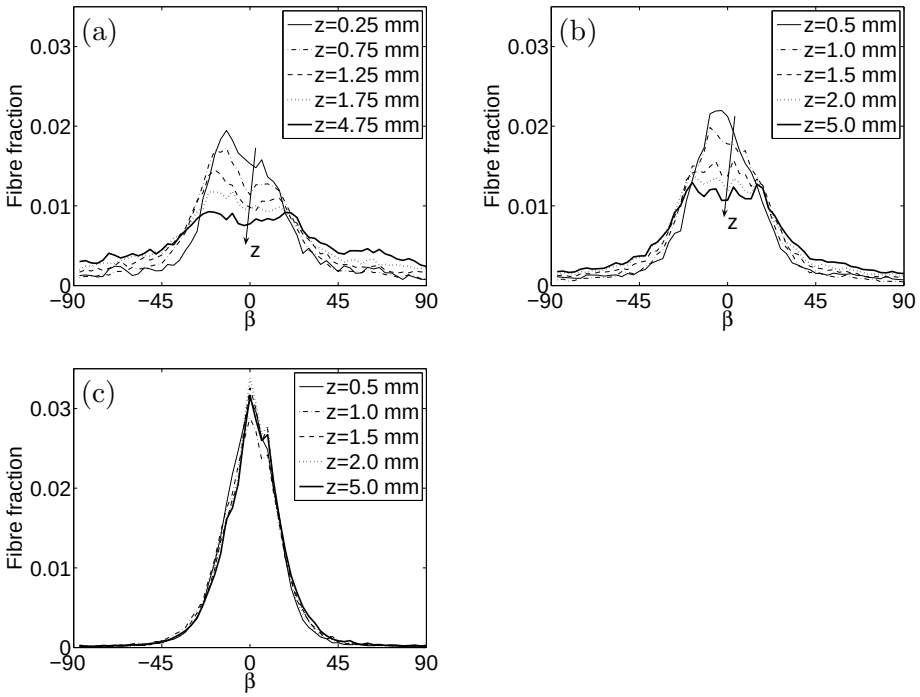

FIGURE 5. The orientation distribution of β for different wall normal positions z at (a) $x = 0.45$ m, (b) $x = 0.25$ m and (c) $x = 0.09$ m.

fibre length and the thickness of the light sheet. Still, also the orientation distribution at $z = 0.5$ mm coincide with the other z-positions. It is possible that the pole vaulting mechanism close to the wall could play a role also here. If the fibres tend to pole vault near the wall few fibres will be located in the region where the shear rate is strongest, but there should still be a small region of high shear in the light sheet where fibres should be present. Therefore this explanation is not completely satisfactorily.

So far attention has only been paid to the shear rate close to the wall and possible intertial effects on the fibre orientation. It was briefly mentioned in the introduction that the main mechanism for the alignment of fibres in a contraction is the streamwise rate-of-strain. The mean streamwise rate-of-strain is not constant in the headbox, but increases downstream. The rate-of-strain in the headbox is the reason for why the orientation distributions turn more anisotropic downstream, which is clearly seen in figure 5. Based on the mean flow velocity, given by the flow rate and geometry of the headbox, the mean

streamwise rate-of-strain is computed to about 1, 4 and 20 s^{-1} for $x = 0.45$, 0.25 and 0.09 m, respectively. Since the strain rate increases downstream this means that the strength of the mechanism for fibre alignment with flow will also grow downstream. This could possibly be the reason to why no difference can be seen in the orientation, even for $z = 0.5$ mm, in figure 5 (c). A speculative explanation would be that the rate-of-strain is now the dominant term influencing the fibre orientation and that other effects, whether it being velocity fluctations, fluid inertia or something else, are small in comparison.

4. Concluding remarks

The fibre orientation has been studied experimentally close to one of the walls of a laboratory scale headbox. The flow rates in the experiments result in jet velocities which are comparable to velocities in industrial paper machines. Only low concentrations were studied due to optical issues and fibre-fibre interactions are therefore likely to have a small effect on the present results. It is concluded, for these low concentrations, that the orientation distribution changes with the distance from the wall for positions in the headbox sufficiently far upstream. The trend is that a more anisotropic distribution is found closer to the wall. This trend was not observed farther downstream at $x = 0.09$ m, where the distribution was seemingly unaffected by presence of the wall. Due to the complexity of the flow only a speculative discussion have been made on possible reasons to why the orientation distribution varies with the wall normal distance. Fluid velocity fluctuations and their dependence on z have been discussed briefly. Also, the fibre dynamics in shear flows and the effect of fluid inertia have been addressed.

References

Aidun, C. K. & Kovacs, A. E. 1995 Hydrodynamics of the forming section: the origin of nonuniform fiber orientation. *Tappi J.* **78** (11), 97–106.

Asplund, G. & Norman, B. 2004 Fibre orientation anisotropy profile over the thickness of a headbox jet. *J. Pulp Paper Sci.* **30** (8), 217–221.

Brown, M. L. 2005 Dynamics of rigid fibres in a planar converging channel. PhD thesis, Georgia Institute of Technology, Atlanta.

Carlsson, A., Lundell, F. & Söderberg, L. D. 2007 Fiber orientation control related to papermaking. *J. Fluids Eng.* **129** (4), 457–465.

Carlsson, A., Lundell, F. & Söderberg, L. D. 2009 Evaluation of steerable filter for detection of fibres in flowing suspensions. Manuscript in preparation.

Carlsson, A., Söderberg, L. D. & Lundell, F. 2008 Fibre orientation in the boundary layers of a planar converging channel. *PaperCon'08 - TAPPI/PIMA/Coating Conference, Dallas* .

Ding, E.-J. & Aidun, C. K. 2000 The dynamics and scaling law for particles suspended in shear flow with inertia. *J. Fluid Mech.* **423**, 317–344.

Freeman, W. T. & Adelson, E. H. 1991 The design and use of steerable filters. *IEEE T. Pattern Anal.* **13** (9), 891–906.

Gavze, E. & Shapiro, M. 1997 Particles in a shear flow near a solid wall: Effect of nonspherity on forces and velocities. *Int. J. Multiphase Flow* **23** (1), 155–182.

Holm, R. & Söderberg, D. 2007 Shear influence on fibre orientation. *Rheol. Acta* **46**, 721–729.

Hsu, R. & Ganatos, P. 1989 The motion of a rigid body in viscous fluid bounded by a plane wall. *J. Fluid Mech.* **207**, 29–72.

Hsu, R. & Ganatos, P. 1994 Gravitational and zero-drag motion of a spheroid adjacent to an inclined plane at low reynolds number. *J. Fluid Mech.* **268**, 267–292.

Hyensjö, M., Dahlkild, A., Krochak, P., Olson, J. & Hämäläinen, J. 2007 Modelling the effect of shear flow on fibre orientation anisotropy in a planar contraction. *Nordic Pulp Paper Res. J.* **22** (3).

Jacob, M. & Unser, M. 2004 Design of steerable filters for feature detection using canny-like criteria. *IEEE T. Pattern Anal.* **26** (8), 1007–1019.

Jeffery, G. B. 1922 The motion of ellipsoidal particles immersed in a viscous fluid. *Proc. Roy. Soc. London A* **102** (715), 161–179.

Kerekes, R. J. & Schell, C. J. 1992 Characterization of fibre flocculation regimes by a crowding factor. *J. Pulp and Paper Sci.* **18** (1), J32–J38.

Krushkal, E. M. & Gallily, I. 1988 On the orientation distribution function of non-spherical aerosol particles in a general shear flow - II. The turbulent case. *J. Aerosol Sci.* **19** (2), 197–211.

Moretti, P. M. & Kays, W. M. 1965 Heat transfer to a turbulent boundary layer with varying free-stream velocity and varying surface temperature - an experimental study. *Int. J. Heat Mass Transfer* **8**, 1187–1202.

Moses, K. B., Advani, S. G. & Reinhardt, A. 2001 Investigation of fiber motion near solid boundaries in simple shear flow. *Rheol. Acta* **40**, 296–306.

Nordström, B. 2003*a* Effects of headbox tube design and flow rate on formation and other sheet properties in twin-wire roll forming. *Nordic Pulp Paper Res. J.* **18** (3), 296–302.

Nordström, B. 2003*b* Effects of pulp type and headbox design on anisotropy and other sheet properties in twin-wire forming. *Nordic Pulp Paper Res. J.* **18** (3), 288–295.

Olson, J. 1998 Analytic estimate of the fibre orientation distribution in a headbox flow. *Nordic Pulp Paper Res. J.* **17** (3), 302–306.

Olson, J., Frigaard, I., Chan, C. & Hämäläinen, J. P. 2004 Modeling a turbulent fibre suspension flowing in a planar contraction: The one-dimensional headbox. *Int. J. Multiphase Flow* **30**, 51–66.

Olson, J. & Kerekes, R. 1998 The motion of fibres in turbulent flow. *J. Fluid Mech.* **17**, 47–64.

Parsheh, M. 2001 Flow in contractions with application to headboxes. PhD thesis, Royal Institute of Technology, Stockholm, Sweden.

Parsheh, M., Brown, M. L. & Aidun, C. K. 2005 On the orientation of stiff fibres suspended in turbulent flow in a planar contraction. *J. Fluid Mech.* **545**, 245–269.

Parsheh, M., Brown, M. L. & Aidun, C. K. 2006*a* Investigation of closure approximations for fiber orientation distribution in contracting turbulent flow. *J. Non-Newtonian Fluid Mech.* **136**, 38–49.

Parsheh, M., Brown, M. L. & Aidun, C. K. 2006*b* Variation of fiber orientation in turbulent flow inside a planar contraction with different shapes. *Int. J. Multiphase Flow* **32**, 1354–1369.

Pozrikidis, C. 2005 Orbiting motion of a freely suspended spheroid near a plane wall. *J. Fluid Mech.* **541**, 105–114.

Qi, D. & Luo, L. S. 2003 Rotational and orientational behaviour of three-dimensional spheroidal particles in couette flows. *J. Fluid Mech.* **477**, 201–213.

Schlichting, H. 1979 *Boundary layer theory*, 7th edn, 166–168. McGraw-Hill.

Stover, C. A. & Cohen, C. 1990 The motion of rodlike particles in the pressure-driven flow between flat plates. *Rheol. Acta* **29**, 192–203.

Subramanian, G. & Koch, D. L. 2005 Inertial effects on fibre motion in simple shear flow. *J. Fluid Mech.* **535**, 383–414.

Sundararajakumar, R. R. & Koch, D. L. 1997 Structure and properties of sheared fiber suspensions with mechanical contacts. *J. Non-Newtonian Fluid Mech.* **73**, 205–239.

Talamelli, A., Fornaciari, N., Westin, K. J. A. & Alfredsson, P. H. 2002 Experimental investigation of streaky structures in a relaminarizing boundary layer. *J. Turbulence* **3** (018).

Ullmar, M. 1998 On fibre alignment mechanisms in a headbox nozzle. Licentiate thesis, Royal Institute of Technology, Stockholm, Sweden.

Warnack, D. & Fernholz, H. H. 1998 The effects of a favourable pressure gradient and of the reynolds number on an incompressible axisymmetric turbulent boundary layer. Part 2. The boundary layer with relaminarization. *J. Fluid Mech.* **359**, 357–381.